16th World Conference on Earthquake, 16WCEE 2017
Santiago Chile, January 9th to 13th 2017
Paper N° 4081
Registration Code: S-N1464736124

DESIGN FLOOR SPECTRA FOR LINEAR AND NONLINEAR SDOF OSCILLATORS

S. Kasinos [1], A. Palmeri [2], M. Lombardo [3]

[1] PhD Candidate, School of Civil & Building Engineering, Loughborough University, UK, S.Kasinos@Lboro.ac.uk
[2] Senior Lecturer, School of Civil & Building Engineering, Loughborough University, UK, A.Palmeri@Lboro.ac.uk and Dynamics.Structures@Gmail.com
[3] Senior Lecturer, School of Civil & Building Engineering, Loughborough University, UK, M.Lombardo@Lboro.ac.uk

Abstract

The seismic analysis and design of secondary attachments to buildings or industrial facilities is a topic of broad engineering interest, increasingly attracting the attention of researchers and practitioners. Examples of secondary systems include suspended ceilings and non-structural walls, piping systems and antennas, storage tanks, electrical transformers and glass façades. Although not part of the load bearing structure, their significance stems from the survivability requirement in the aftermath of a seismic event and their vast contribution to the overall construction costs. Nevertheless, past earthquakes have demonstrated that current methods for the seismic analysis and design of secondary structures lack the necessary rigor and robustness, resulting in expensive and often unreliable solutions. Secondary systems can be highly sensitive to accelerations and inter-story drifts, and their seismic performance is influenced by the primary-secondary dynamic interaction. In many situations however, the mass of the secondary system may be much lower than the mass of the floor at which it is connected and therefore a cascade approach is admissible. If the secondary system can be realistically modeled as a single-degree-of-freedom (SDoF) system, then the floor response spectra could be a powerful tool for quantifying its seismic response.

In this study, the performance of light secondary systems is examined in presence of uncertainties in the seismic input. A set of principal axes of ground shaking is initially identified and an ensemble of bi-directional time series is generated. The response of a set of SDoF secondary oscillators (i.e. linear, Bouc-Wen, sliding and rocking) attached to a representative primary structure is then investigated and their design spectra are established. As demonstrated with Monte Carlo simulations for the selected case study, the angle of seismic incidence causes the highest variations in the engineering demand parameters for the sliding oscillators, while the elasto-plastic oscillator with the Bouc-Wen model experiences the least variations. Furthermore, investigations at different elevations show higher variations in the sliding and linear oscillators, depending on the seismic input. As expected, the viscous damping ratio is found to significantly influence the response of secondary systems vibrating close to the fundamental frequency of the primary structure. Moreover, the peak response of sliding oscillators is shown to be a smooth function of the sliding friction coefficient, while the rocking spectra, due to the strong nonlinear dynamics of the rocking blocks, are characterized by large values of the coefficient of variations.

Keywords: nonlinear oscillators; nonstationary processes; nonstructural components; secondary structures; stochastic models

1. Introduction

The response analysis of secondary attachments and content, such as fittings, piping and equipment, plays a critical role in the seismic assessment of buildings structures. As a matter of fact, such building components are termed "secondary" simply because they are not part of the "primary" load-bearing system. Despite their name, however, their significance is far from being marginal, as their monetary value typically exceeds the cost of the bare structure, while their failure may result in tremendous losses, in terms of repair costs, interruption of services, as well as injuries and even deaths [1, 2]. Secondary systems can be connected to the primary structure in multiple attachment points (e.g. fire staircases), or quite often just at a single location (e.g. tanks and antennas on the rooftop). In the latter case,

floor spectra represent a powerful tool to quantify their expected performance under design earthquake scenarios. This approach is only tenable under the "light" secondary system approximation [3] in which: (*i*) the mass of the secondary is significantly less than the mass of the floor at which it is connected, meaning that the feedback action on the primary structure is negligible; (*ii*) its dynamics can be approximated with a single-degree-of-freedom (SDoF) oscillator model, which can be either linear or nonlinear. Furthermore, depending on the level of the seismic input and the characteristics of the building structure, a linear or nonlinear model can be adopted for the primary structure.

In the context of probabilistic performance-based earthquake engineering (PBEE), uncertainty characterizing the performance of structures must be adequately quantified. In particular, the uncertainty in the ground motion often exceeds the one associated with the structure [4]. Hazard models capable of capturing characteristics encountered in transient seismic signals are thus of interest. The use of recorded seismic accelerograms is accompanied with a main shortcoming, i.e. they represent only a single realization of the probabilistic hazard. To circumvent this, the use of scaled recorded motions has been proposed, but concerns have been raised, as they may render unphysical characteristics [4]. More recently, several techniques have been put forward for the generation of artificial ground motions, whose characteristics aim to match the ones of target accelerograms, including various wavelet-based methods (e.g. [5] and [6]) as well as the ones evolved from the filtered white noise process [7, 8]. As an example of the latter, a model proposed by Rezaeian and Der Kiureghian [9, 10] is particularly appealing, encompassing completely separable temporal and spectral non-stationarities. The model has been further extended to multi-component simulation [11] based on the work of Penzien and Watabe [12], who identified a set of principal axes along which the orthogonal components of a ground motion can be considered as statistically uncorrelated.

Structures subjected to the simultaneous components of ground acceleration may exhibit unfavourable demands in numerous angles of attack. Accordingly, given an engineering demand parameter (EDP), the critical angle governing the response of a primary system may be estimated by combining the contributions of the ground motion components [13]. This becomes particularly cumbersome in the case of secondary systems, as the critical angle of seismic incidence is an implicit function of the secondary system's angle relative to the primary, its mechanical properties and the EDP used for response assessment [14].

To the author's best knowledge no studies have been reported in the literature where the response of secondary systems is investigated in presence of uncertainties in a multi-dimensional ground motion model. Prompted by the significance and relative fragility of secondary systems, the authors have recently investigated the propagation of uncertainty from the modal properties of the primary structure to the seismic performance of secondary oscillators [15]. In this paper, the effect of uncertainties in a bi-directional seismic input to the response of light secondary subsystems is examined. More specifically, a set of principal axes is first identified for a near-field and a far-field earthquake record. The stochastic model originally established in [9] is then adopted and a number of bi-directional signals are synthetically generated via Monte Carlo simulations with the same non-stationary characteristics as the parent accelerograms. This ensemble is then used for various angles of incidence for the major principal direction of the seismic input, with linear dynamic analyses carried out on a primary structure attached to a set of linear and nonlinear (Bouc-Wen, sliding, rocking) secondary SDoF oscillators. The design floor spectra are finally established, and the effects of the key parameters are analyzed and discussed.

2. Governing Equations

2.1 Principal axes

Let us consider the case of a ground motion record defined through a pair of horizontal orthogonal components. The correlation coefficient over the total duration of motion can then be expressed as:

$$\rho_{a_1(t)a_2(t)} = \frac{\int_{t_0}^{t_n} a_1(t)a_2(t)\,\mathrm{d}t}{\sqrt{\int_{t_0}^{t_n} a_1(t)^2\,\mathrm{d}t \int_{t_0}^{t_n} a_2(t)^2\,\mathrm{d}t}}, \quad (1)$$

where t_0, t_n are the initial and final time instants and $a_1(t)$, $a_2(t)$ the associated acceleration time series, respectively [11]. Following the work of Penzien and Watabe [12], a set of principal axes η and ξ exists (see

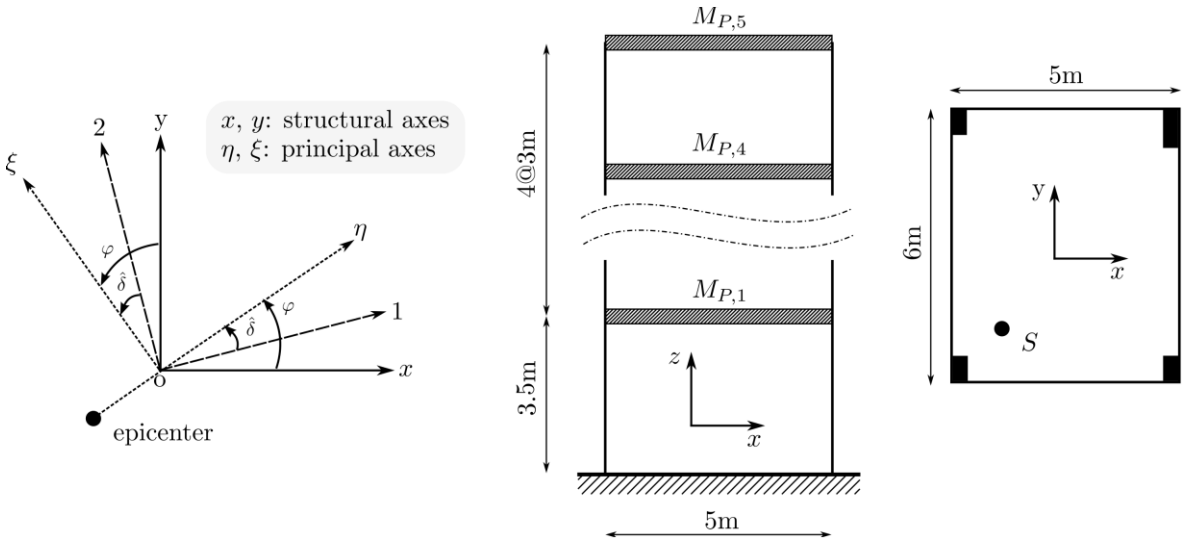

Fig. 1 - Rotation of orthogonal horizontal components (left), and structural frame model (right)

Figure 1, left) along which the components are statistically uncorrelated. Accordingly, introducing the rotation angle δ in the range 0° to 90° and adopting the following orthogonal transformation:

$$\boldsymbol{a}_p(\delta, t) = \mathbf{R}(\delta) \cdot \boldsymbol{a}(t)\,, \tag{2}$$

one can derive an angle $\hat{\delta}$ where the components are principal, such that $\rho_{a_{1,p}(\hat{\delta},t),a_{2,p}(\hat{\delta},t)} = 0$, where $\boldsymbol{a}(t)$ and $\boldsymbol{a}_p(\delta, t)$ are arrays listing the "as-recorded" and "rotated" acceleration time series of the horizontal components, respectively, and $\mathbf{R}(\delta)$ is a rotation matrix defined as:

$$\boldsymbol{a}_p(\delta, t) = \begin{bmatrix} a_{1,p}(\delta, t) \\ a_{2,p}(\delta, t) \end{bmatrix}, \quad \mathbf{R}(\delta) = \begin{bmatrix} \cos(\delta) & \sin(\delta) \\ -\sin(\delta) & \cos(\delta) \end{bmatrix}, \quad \boldsymbol{a}(t) = \begin{bmatrix} a_1(t) \\ a_2(t) \end{bmatrix}. \tag{3}$$

2.2 Stochastic ground motion model

Given the statistically independent principal components of the target accelerogram $\boldsymbol{a}_p(\hat{\delta}, t)$, a stochastic ground motion model can then be used to simulate bi-directional time series with temporal and spectral nonstationarities. Adopting the formulation proposed by Rezaeian and Der Kiureghian [9, 11] the continuous form of a Gaussian ground acceleration process is defined by:

$$x_r(t) = q(t, \boldsymbol{\kappa}_r)\left\{\frac{1}{\sigma_{hr}(t)}\int_{-\infty}^{t} h[t-\tau, \boldsymbol{\lambda}_r(\tau)] w_r(\tau)\,\mathrm{d}t\right\}, \quad r = 1, 2\ , \tag{4}$$

in which $x_r(t)$ is the acceleration process of the rth component; $q(t, \boldsymbol{\kappa}_r)$ is a deterministic time-modulating function, depending on a set of parameters $\boldsymbol{\kappa}_r$ that defines its intensity and shape; $w_r(\tau)$ is a Gaussian white-noise process; $h[t-\tau, \boldsymbol{\lambda}_r(\tau)]$ is the impulse-response function (IRF) of a filter with parameters $\boldsymbol{\lambda}_r(\tau)$ accounting for the spectral nonstationarity; $\sigma_{hr}^2(t) = \int_{-\infty}^{t} h^2[t-\tau, \boldsymbol{\lambda}_r(\tau)]\,\mathrm{d}t$ is the variance of the integral process. The term in the curly brackets therefore represents a filtered white-noise process of unit variance and $q(t, \boldsymbol{\kappa}_r)$ is equal to the standard deviation of the process, fully defining the temporal nonstationarity.

A piecewise modulating function is adopted:

$$q(t, \boldsymbol{\kappa}) = \begin{cases} \sigma_{\max}\left(\dfrac{t-T_0}{T_1-T_0}\right)^2 & \text{if } T_0 < t \le T_1 \\ \sigma_{\max} & \text{if } T_1 < t < T_2 \\ \sigma_{\max}\exp[-\gamma_1(t-T_2)^{\gamma_2}] & \text{if } T_2 \le t \\ 0 & \text{otherwise} \end{cases} \tag{5}$$

with the parameter set $\boldsymbol{\kappa} = (T_0,\ T_1,\ T_2, \sigma_{\max}, \gamma_1, \gamma_2)$ to be identified, satisfying $T_0 < T_1 \leq T_2$ and $\sigma_{\max}, \gamma_1, \gamma_2 > 0$. Accordingly, T_0 represents the initiation time of the process, while T_1, T_2 denote the start and end of the strong-motion phase, with maximum standard deviation $\sigma_{\max}$, and γ_1, γ_2 are parameters controlling the decaying amplitude.

The filter IRF is chosen as:

$$h[t-\tau, \boldsymbol{\lambda}(\tau)] = \begin{cases} \dfrac{\omega_f(\tau)}{\sqrt{1-\zeta_f^2(\tau)}} \exp\left[-\zeta_f(\tau)\omega_f(\tau)(t-\tau)\right] \sin\left[\omega_f(\tau)\sqrt{1-\zeta_f^2(\tau)}(t-\tau)\right] & \text{if } \tau \leq t \\ 0 & \text{otherwise} \end{cases} \tag{6}$$

corresponding to the pseudo-acceleration response of a linear SDoF oscillator where the parameter set $\boldsymbol{\lambda}(\tau) = \left(\omega_f(\tau), \zeta_f(\tau)\right)$ lists the time-varying frequency and damping ratio. Herein, based on [10], a linear function is adopted for the frequency and a piece-wise function for the damping:

$$\omega_f(\tau) = \omega_0 - (\omega_0 - \omega_n)\frac{\tau}{t_n}; \quad \zeta_f(\tau) = \begin{cases} \zeta_1 & \text{if } 0 \leq \tau \leq t_1 \\ \vdots & \vdots \\ \zeta_n & \text{if } t_{n-1} < \tau \leq t_n \end{cases} \tag{7}$$

where ω_0 and ω_n are the initial and final filter frequencies ($\omega_0 > \omega_n$), t_n is the duration of motion, and $\zeta_1, \dots, \zeta_n$ are damping coefficients to be identified for the target motion.

Denoting $t_i,\ i = 0,1, \dots n$ as distinct time instants with time step Δt and letting $k = \text{int}(t/\Delta t)$ for $0 < t \leq t_n$, the discretized form of the stochastic model in Eq. (4) reads:

$$\hat{x}_r(t) = q(t, \boldsymbol{\kappa}_r) \sum_{i=1}^{k} \left\{ s_i\left(t, \boldsymbol{\lambda}_r(t_i)\right) v_{i,r} \right\}, \quad t_k \leq t < t_{k+1}, \quad r = 1,2\ , \tag{8}$$

in which $v_{i,r}$ are standard normal random variables used to define the white-noise process and $s_i\left(t, \boldsymbol{\lambda}_r(t_i)\right)$ are deterministic basis functions, where:

$$s_i\left(t, \boldsymbol{\lambda}_r(t_i)\right) = \frac{h[t-t_i, \boldsymbol{\lambda}_r(t_i)]}{\sqrt{\sum_{j=1}^{k} h^2\left[t-t_j, \boldsymbol{\lambda}_r(t_j)\right]}}, \quad t_k \leq t < t_{k+1}, \quad i = 1, \dots, k, \quad r = 1,2\ , \tag{9}$$

Once the model parameters are identified, the random variables $v_{i,r}$, and the basis functions $s_i\left(t, \boldsymbol{\lambda}_r(t_i)\right)$ are used to generate realisations of the processes in Eq. (8).

Given the simulated process, a critically damped high pass filter is adopted adjusting the low frequency content of the model, to ensure zero residual displacement and velocity. The corrected acceleration record $\ddot{y}_r(t)$ is finally obtained as the response of:

$$\ddot{y}_r(t) + 2\omega_c \dot{y}_r(t) + \omega_c^2 y_r(t) = \hat{x}_r(t), \quad r = 1,2\ , \tag{10}$$

where ω_c is the filter frequency ($\omega_c \approx 0.2 - 0.4\pi$ rad/s).

Notably: (*i*) the statistically independent processes $w_1(\tau)$, $w_2(\tau)$ account for the stochasticity in the model; (*ii*) both temporal and spectral nonstationarities are considered through the parameter sets $\boldsymbol{\kappa}_r$ and $\boldsymbol{\lambda}(\tau)$, respectively.

2.3 Seismic incidence orientation

Response assessment of structures subjected to bi-directional seismic action requires determination of the critical angle of seismic incidence. Accordingly, let us define φ as the counter clockwise angle in the range 0° to 180° between the reference axes of the structure (x and y in Figure 1, left) and the principal axes (η, ξ) of the seismic input. Utilizing the transformation:

$$\ddot{\boldsymbol{u}}_g(\varphi, t) = \mathbf{R}(\varphi) \cdot \boldsymbol{a}_y(t)\ , \tag{11}$$

a set of horizontal ground acceleration $\ddot{\boldsymbol{u}}_g(\varphi,t)$ is obtained along the structural axes, where $\boldsymbol{a}_y(t)$ collects the filtered processes of the two components (see Eq. (10)), such that:

$$\boldsymbol{a}_y(t) = \begin{bmatrix}\ddot{y}_1(t)\\ \ddot{y}_2(t)\end{bmatrix}; \quad \ddot{\boldsymbol{u}}_g(\varphi,t) = \begin{bmatrix}\ddot{u}_{g,1}(\varphi,t)\\ \ddot{u}_{g,2}(\varphi,t)\end{bmatrix}. \tag{12}$$

2.4 Linear Primary System

Let's consider the case of a deterministic primary-secondary system. If the secondary one is assumed to be "light" [3], i.e. its mass m_S is much less than the mass of the primary M_P ($m_S \ll M_P$), a cascade-type approach is admissible. Accordingly, the two systems are decoupled and sequentially analysed. Initially, the seismic response of the primary system is determined neglecting the feedback of the secondary, with the response of the latter successively being evaluated at the points of attachment (i.e. no primary-secondary interaction is taken into account).

The seismic motion of a multi-degree-of-freedom (MDoF) primary system within the linear-elastic range is governed by:

$$\mathbf{M}\cdot\ddot{\boldsymbol{u}}(\varphi,t) + \mathbf{C}\cdot\dot{\boldsymbol{u}}(\varphi,t) + \mathbf{K}\cdot\boldsymbol{u}(\varphi,t) = -\mathbf{M}\cdot\boldsymbol{\tau}\cdot\ddot{\boldsymbol{u}}_g(\varphi,t)\,, \tag{13}$$

where $\mathbf{M}$, $\mathbf{C}$ and $\mathbf{K}$ are matrices of mass, equivalent viscous damping and elastic stiffness, respectively; $\boldsymbol{u}(\varphi,\mathrm{t})$ is the array collecting the degrees of freedom (DoFs) of the system; $\boldsymbol{\tau}$ is a vector of seismic incidence.

The equations of motion can be projected to the modal space, reducing the size of the dynamic problem from m_1 (system's DoFs) to $m_2 \le m_1$ (the number of modes retained within the analysis). This requires solving the real-valued eigenproblem:

$$\mathbf{M}\cdot\boldsymbol{\Phi}\cdot\boldsymbol{\Omega}^2 = \mathbf{K}\cdot\boldsymbol{\Phi}\,, \tag{14}$$

where $\boldsymbol{\Phi} = [\boldsymbol{\phi}_1 \cdots \boldsymbol{\phi}_{m_2}]$ is the normalized modal matrix (i.e. $\boldsymbol{\Phi}^{\mathsf{T}}\cdot\mathbf{M}\cdot\boldsymbol{\Phi} = \mathbf{I}_{m_2}$), $\mathbf{I}_{m_2}$ being the identity matrix of size *m*; and $\boldsymbol{\Omega} = \mathrm{diag}\{\omega_1 \cdots \omega_{m_2}\}$ the diagonal spectral matrix. Accordingly, the dynamic response can be expressed as the sum of modal contributions:

$$\boldsymbol{u}(\varphi,\mathrm{t}) = \boldsymbol{\Phi}\cdot\boldsymbol{q}(\varphi,t), \tag{15}$$

where $\boldsymbol{q}(\varphi,\mathrm{t}) = \{q_1(\varphi,t)\cdots q_{m_2}(\varphi,t)\}^{\mathsf{T}}$ is the array collecting the modal coordinates, ruled by the equation of motion in the modal space:

$$\ddot{\boldsymbol{q}}(\varphi,\mathrm{t}) + 2\zeta\,\boldsymbol{\Omega}\cdot\dot{\boldsymbol{q}}(\varphi,\mathrm{t}) + \boldsymbol{\Omega}^2\cdot\boldsymbol{q}(\varphi,\mathrm{t}) = \mathbf{p}\cdot\ddot{\boldsymbol{u}}_g(\varphi,t)\,, \tag{16}$$

in which ζ is the viscous damping ratio of the primary structure and:

$$\mathbf{p} = -\boldsymbol{\Phi}^{\mathsf{T}}\cdot\mathbf{M}\cdot\boldsymbol{\tau}\,. \tag{17}$$

2.5 Secondary oscillators

2.5.1 Linear and nonlinear Bouc-Wen restoring force

The equation of motion of a linear SDoF secondary system is expressed as:

$$\ddot{u}_S(\varphi,t) + 2\zeta_S\omega_S\,\dot{u}_S(\varphi,t) + f_R(\varphi,t) = -\ddot{u}_{P,i}^{(\mathrm{a})}(\varphi,t)\,, \tag{18}$$

where ω_S and ζ_S are the associated natural vibration frequency and damping ratio, respectively, while $\ddot{u}_{P,i}^{(\mathrm{a})}(\varphi,t) = \ddot{u}_{P,i}(\varphi,t) + \ddot{u}_{g,i}(\varphi,t)$ is the unidirectional absolute acceleration response of the primary structure at the position of attachment. For a linear system, the restoring force is $f_R(\varphi,t) = \omega_S^2\,u_S(\varphi,t)$; alternatively if the subsystem is considered nonlinear $f_R(\varphi,t)$ becomes an implicit function of the deformation. Adopting the well-known Bouc-Wen model [16, 17], $f_R(\varphi,t)$ can then be posed in the form:

$$f_R(\varphi,t) = \psi\,\omega_S^2 u(\varphi,t) + (1-\psi)\varepsilon\,z(\varphi,t)\,, \tag{19}$$

where ψ is the ratio of post-yield to pre-yield stiffness (setting $\psi = 0$ corresponds to an elastic-perfectly plastic case while $\psi = 1$ leads to the linear one); $\varepsilon = f_y/m$ is a measure of the ground acceleration required for the system to yield; $z(\varphi, t)$ is a dimensionless hysteretic variable, ruled by:

$$\dot{z}(t) = \frac{\omega_S^2}{\varepsilon}\{1 - |z|^n(\beta + \gamma\ \mathrm{sgn}[\dot{u}(\varphi,t)\ z(\varphi,t)])\}\ \dot{u}(\varphi,t)\ , \tag{20}$$

in which β, γ, n are dimensionless parameters controlling the shape of the hysteresis model and $\mathrm{sgn}(.)$ is the signum function.

2.5.2 Sliding block

The case of a rigid-perfectly plastic SDoF system can be considered as the limiting case ($\omega_S \to +\infty$ and $n \to +\infty$) of the above restoring force, where the equation of motion becomes:

$$\ddot{u}_S(\varphi,\mathrm{t}) = \begin{cases} -\ddot{u}_{P,i}^{(\mathrm{a})}(\varphi,\mathrm{t}) - \ \mu_S\ g\ \mathrm{sgn}\left(\dot{u}_{P,i}^{(\mathrm{a})}(\varphi,\mathrm{t})\right) & \text{if } \left|\ddot{u}_{P,i}^{(\mathrm{a})}(\varphi,\mathrm{t})\right| > \mu_s\ g \\ 0 & \text{otherwise} \end{cases} \tag{21}$$

in which μ_S is the coefficient of sliding friction of the secondary system and g is the acceleration due to gravity. Notably, the above equation corresponds to a pure slide mode and is the same as Eq. (2) presented in [18].

2.5.3 Rocking block

If the system undergoes pure rocking motion ($\mu_S \to \infty$), the equation governing the response of a free-standing subsystem is then ruled by:

$$\ddot{\theta}_S(\varphi,t) = -p^2\left\{\sin\big(\alpha\ \mathrm{sgn}[\theta_S(\varphi,t)] - \theta_S(\varphi,t)\big) + \frac{\ddot{u}_{P,i}^{(\mathrm{a})}(\varphi,\mathrm{t})}{g}\cos\big(\alpha\ \mathrm{sgn}[\theta_S(\varphi,t)] - \theta_S(\varphi,t)\big)\right\}\ , \tag{22}$$

and

$$\dot{\theta}_S^{\mathrm{a}} = e_{\max}\ \dot{\theta}_S^{\mathrm{b}}, \qquad e_{\max} = \frac{1 + s\cos(2\alpha)}{1+s}, \tag{23}$$

in which $\theta_S(\varphi,t)$ is the rotation response of the block; slenderness angle α and the parameter p characterize its dynamics (e.g. for a rectangular block, $p = \sqrt{3g/(4R)}$; furthermore, $p \approx 2\ \mathrm{rad/s}$ for an electrical transformer), along with the coefficient of restitution $e = e_{\max}$, which accounts for the reduction in the angular velocity before ($\dot{\theta}_S^{\mathrm{b}}$) and after ($\dot{\theta}_S^{\mathrm{a}}$) an impact, when θ_S changes sign (again, for a rectangular block, $e_{\max} = 1 - 3\sin^2(\alpha)/2$, R being half the block's diameter and the shape factor is $s = 3$) [19, 20, 21].

3. Application

In order to assess the seismic response of secondary structures subjected to the simultaneous action of orthogonal horizontal components, a representative case study has been numerically investigated. Figure 1 (right), shows a MDoF primary system comprising of a 5-storey single-bay moment-resisting frame, being irregular in plan and elevation, with position *S* denoting the attachment point of a light SDoF secondary system of unit mass at top story (chosen as representative), modeled as (*i*) linear, (*ii*) Bouc-Wen, (*iii*) sliding and (*iv*) rocking oscillator. Floors are rigid in plane, while the self-weight and super-dead load constitute the mass source of the structure. The fundamental period of vibration in the direction of interest x and damping ratio are $T_{\mathrm{P},x} = 0.382s$, $\zeta = 0.05$ for the primary structure and $T_{\mathrm{S}} = 0.9T_{\mathrm{P},x}$, $\zeta_{\mathrm{S}} = 0.02$ for the secondary (cases (*i*) and (*ii*)). The number of modal coordinates retained in the analysis is $m_2 = 5$, chosen such that at least 90% of the modal mass participates in the seismic motion, a criterion set by current codes of practice [22]. The Bouc-Wen parameters are taken as $\psi = 0$, $\beta = \gamma = 0.5$, $n = 5$ representing the case of elastic-perfectly plastic and ε is chosen as a fraction of the response of the equivalent linear oscillator. The friction coefficient is $\mu_S = 0.2$ and the parameters of the rocking oscillator are $\alpha = 0.2\mathrm{rad}$ and $p = 1\mathrm{rad/s}$, while the overturning condition is set as $\theta_S(\varphi,t) = \alpha$.

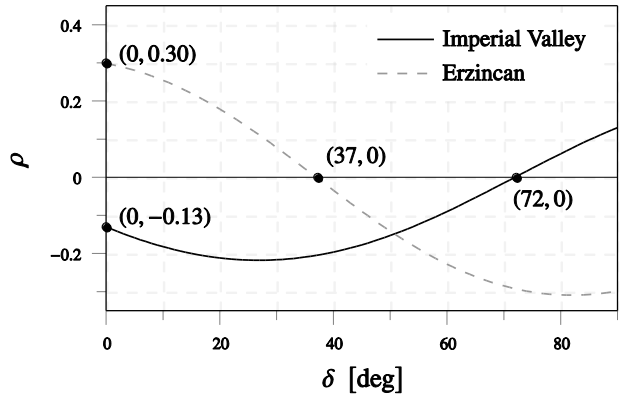

Fig. 2 - Correlation coefficient of orthogonal components.

3.1 Identification of ground motion model parameters

Two recorded accelerograms have been considered, namely El Centro 1940 and Erzincan 1992, chosen as representative candidates for different earthquake scenarios and their principal horizontal components have been identified by examining the correlation coefficient of their as-recorded associated components (see Eqs. (1) and (2)). The parameters of the ground motion model have been obtained based on the procedure described in [10]. In doing so, the modulating function parameters $\boldsymbol{\kappa}_r$ were initially determined, by minimizing the squared difference between the expected cumulative energy of the process and the one of the recorded accelerograms. Given the inter-dependence between the frequency and damping parameters, $\omega_0(\tau)$ and $\omega_n(\tau)$ were first identified over constant values of $\zeta_f(\tau)$, by minimizing the mean-square error of the cumulative expected number of zero-level up-crossings of the process and the target accelerogram. A set of 20 simulations was then used, over a range of damping values $\zeta_f = 0.1,0.2,\ldots,1$ and the slope of the cumulative number of negative maxima plus positive minima of the model process was compared to that of the target motion. To account for the time-variation in the damping ratio, four-segments were used over the total duration of motion. The frequency parameters were then refined according to the damping ratios chosen.

3.2 Numerical analyses

A Monte Carlo simulation (MCS) comprising of a series of linear dynamic analyses has been carried out with $n_{\text{sym}} = 500$ realisations, using the commercial software SAP2000 [23] and the numerical software MATLAB [24], assessing the structural response in presence of uncertainties in the seismic input. The primary structure has been excited by the 2 ground motion records at 12 different angles of seismic incidence per ground motion pair, from 0° to 165° by transforming the time series using Eq. (12) and assigning them in the x and y directions as shown in Figure 1 (left). In doing so, the angle of attack of the secondary systems was assumed the same as the one of the primary.

In a first stage, the stochastic ground motion model is verified by comparing the statistics of the processes to the two target motions considered. In a second stage, the response of the secondary subsystems is examined for different configurations (i.e. different elevations and angles of attack). In a third stage, the influence of various mechanical parameters on the response statistics of the secondary oscillators is investigated and a set of design spectra is presented. Various EDPs were considered, namely: the maximum absolute acceleration ($\max\left\{\ddot{u}_{P,i}^{(\mathrm{a})}(\varphi,t)\right\}$) for the linear primary structure; the maximum relative displacement ($\max\{u_S(\varphi,t)\}$) for the linear, Bouc-Wen and sliding secondary oscillators; and the maximum normalized rotation ($\max\left\{\frac{\theta_S(\varphi,t)}{\alpha}\right\}$) for the rocking block.

3.2.1 Simulated motions

Figure 2 confirms that the correlation coefficient calculated over each pair of components is a smooth function of the rotation angle. For the two earthquakes under consideration, $\rho = 0$ when $\delta = 72°$ and $\delta = 37°$, respectively, and the associated components can be considered as principal. Figure 3 compares the 5% damped elastic response spectra of

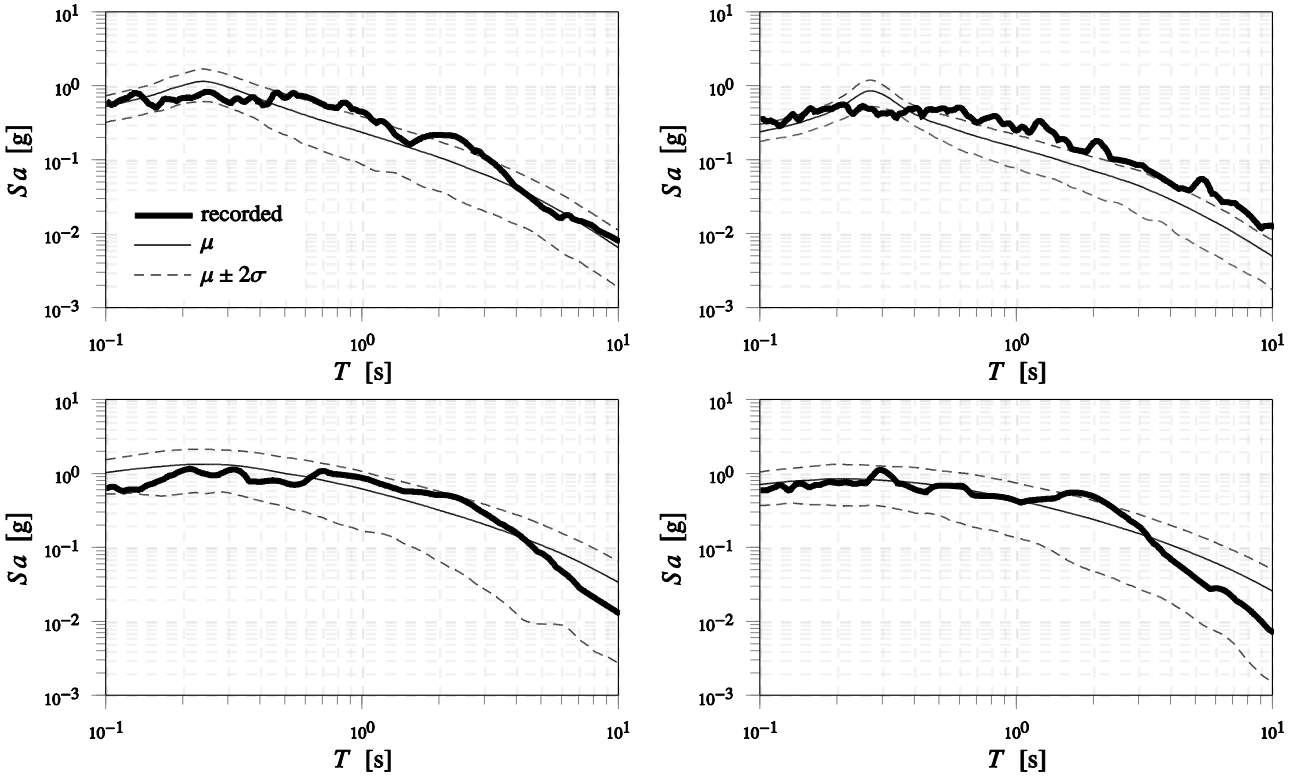

Fig. 3 - Comparison between 5% damped elastic response spectra of recorded and simulated orthogonal components for Imperial Valley (top) and Erzincan (bottom) earthquakes.

the resulting 500 simulated orthogonal components with the recorded ones. Overall, a satisfactory match is observed and thus the simulated motions are exploited to the subsequent stages of the analysis. It is worth mentioning here that the discrepancies seen for the case of Imperial Valley (Fig.3, top) are due to the ground motion possessing multiple dominant periods. Although out of the scope of this study, this can be accounted for through MDoF filter [10].

3.2.2 Elevation and angle of seismic incidence

Following the generation of the simulated ground motions and the evaluation of the seismic response for the primary structure at the points of attachment, our analyses proceed with the cascade dynamic analysis of the four secondary oscillators under consideration. Figure 4 (top) shows the expected values of the EDPs at top level of the MDoF frame as a function of the angle of attack normalized with the respective values of the principal direction (i.e. $\varphi = 0°$). Similar trends are seen in the curves for all cases, with the highest EDPs predicted when $\varphi = 0°$. Highest magnitude reductions are observed at $\varphi = 90°$ for the sliding oscillator (50%) while the lowest are found for the Bouc-Wen (20-25%). Interestingly, for the case of Erzincan the sliding oscillators show reduced sensitivity to the angle of attack of the earthquake, meaning that the latter can be record-dependent.

Figure 4 (2nd row) illustrates the results at different elevations and constant $\varphi = 0°$, normalized with the relevant EDPs at the top level. As expected, in all cases the EDPs increase with the height, due to the dynamic amplification caused by the seismic motion of the primary structure, with the sliding and linear oscillators showing the highest variations. Furthermore, due to their strong nonlinearities, sliding and rocking blocks show high variability between the two earthquakes.

Plotting the normalized EDPs of the secondary oscillators against the normalized EDP of the primary structure at the attachment points (Figure 4, bottom), one can observe that the resulting points tend to lie close to the main diagonal line at 45° for the case of the first record, while they are more scattered for the second record (particularly the data points for the sliding and the rocking blocks). Notably, although a certain degree of correlation is evident between the two EDPs, the variations with the type of nonlinearity and the time-frequency characteristics of the seismic input suggest that further investigations are required to understand how the two seismic responses are related.

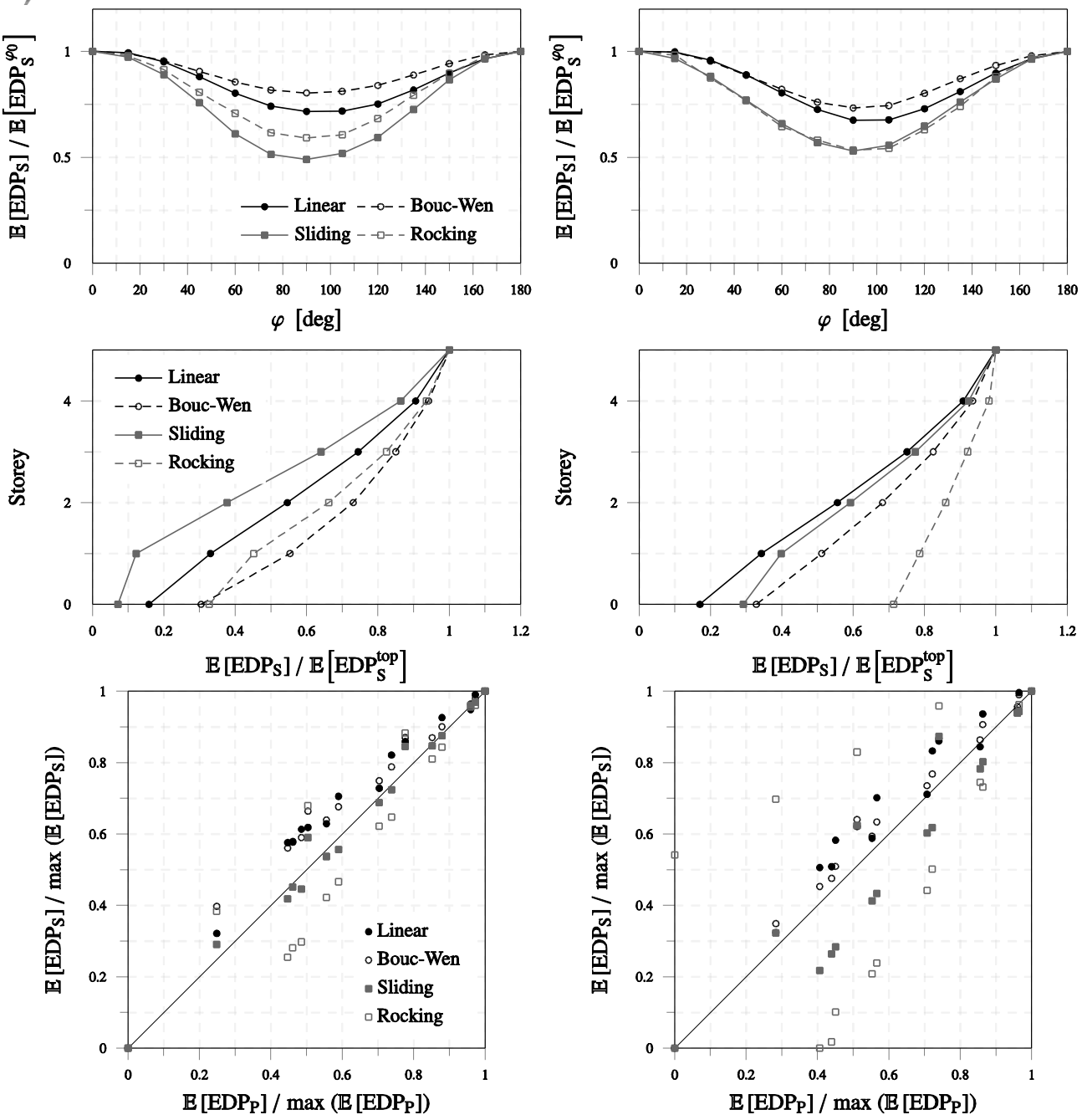

Fig. 4 - Normalized expected EDPs of secondary systems at various angles of attack (top) , elevations (middle), and correlation between secondary-primary normalized expected EDPs due to the simulated motions of the 1940 Imperial Valley (left) and 1992 Erzincan (right) earthquakes.

3.2.3 Response spectra

Finally, the effects of various parameters governing the response of the secondary oscillators are presented in terms of the associated EDPs evaluated at the top level and for different angles of seismic incidence. Figure 5 (top) shows the earthquake spectra for the linear oscillator with two levels of viscous damping ratio. Overall, the expected EDPs and response variance increase with T_S, and an amplification is seen near the resonant period of the primary structure (i.e. $T_S = T_{P,x} = 0.382s$). Increasing the damping ratio ζ_S from 0.02 to 0.05 causes a reduction in the order of 50% for both records. In this case then, an accurate evaluation of the inherent damping of the secondary system appears of utmost importance, especially if the risk of resonant motion exists.

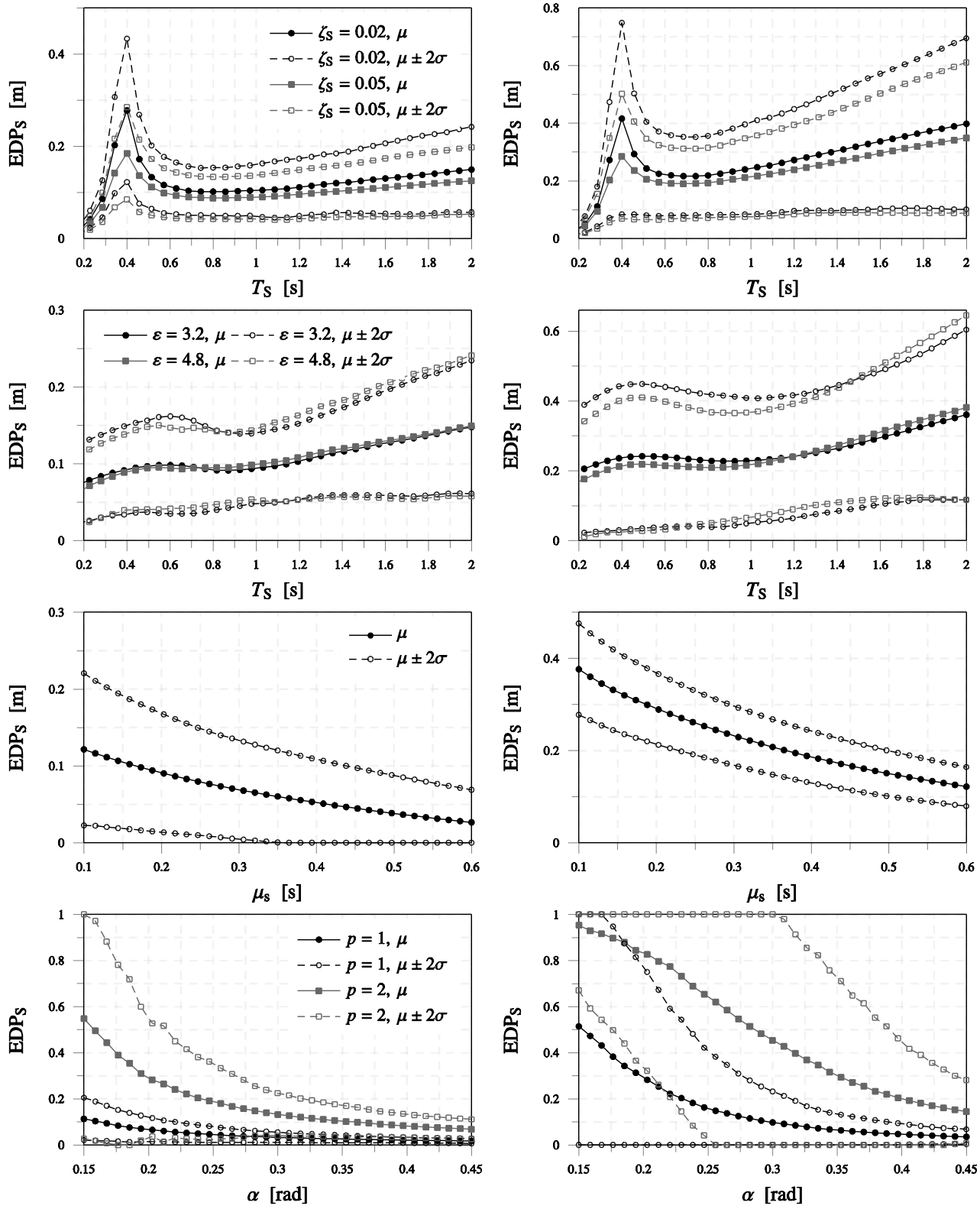

Fig. 5 - Spectra of a linear secondary system with $\zeta_S = 0.02$ and $\zeta_S = 0.05$ (top row), Bouc-Wen secondary system with $\varepsilon = 3.2$ and $\varepsilon = 4.8$ (2nd row), sliding secondary system (3rd row) and rocking secondary system with $p = 1$, 2 rad/s and $\varepsilon_r = 0.5$ (bottom row) when subjected to the simulated motions of the 1940 Imperial Valley (left) and 1992 Erzincan (right) earthquakes.

Figure 5 (2nd row) shows the nonlinear spectra for elastoplastic oscillators with the Bouc-Wen model, considering two values of yielding acceleration ε. As expected, the dynamic amplification seen in the linear system is significantly reduced at $T_S = T_{P,x}$, due to the energy being dissipated in the elastoplastic (frequency-independend) cycles. Furthermore, increasing ε shows a reduction of the seismic response for short periods, while the EDP increases for longer periods.

The sliding spectra are presented in the 3rd row of Figure 5. Smooth curves are observed (i.e. no resonant peaks are seen), with progressively smaller values of EDP and less response variance when the friction coefficient increases. An overall a reduction of about 70% in the EDPs is shown for the two earthquakes.

Finally, the last row of Figure 5 shows the rocking spectra for two values of the dynamic parameter p and the two earthquake records. Overall, higher EDPs are predicted for the near-field case of Erzincan. As shown, the smaller the slenderness angle α and the higher the dynamic parameter p, the more likely the subsystem is to overturn and the higher the variance of the seismic response. In particular, reducing the dynamic parameter p from 2 to 1 rad/s can reduce the expected value of the EDP, θ_{max}/α, up to about 80%. It therefore appears that, given a design earthquake scenario, the choice of the dynamic parameter in conjunction with the slenderness may be critical on the seismic response of secondary rocking systems.

4. Conclusions

The stochastic seismic response of light secondary subsystems was investigated in presence of uncertainties in simultaneous bi-directional ground motions. First, a set of principal axes has been identified for a near-field and a far-field earthquake record. An ensemble of bi-directional time series was then generated and the response of various secondary structures modeled either as linear or nonlinear SDoF oscillators (i.e. linear, Bouc-Wen, sliding and rocking) was quantified for various configurations (different elevations and angles of attack). The design spectra were then established, allowing the quantification of the seismic performance for various subsystems under the selected design scenarios. The following conclusions can be drawn:

(1) The angle of seismic incidence was shown to cause the highest variations in the EDP of the sliding oscillator (about 50%) and it least affected the Bouc-Wen oscillator (about 20-25%). Furthermore, investigation on the response of subsystems at different elevations showed higher variations in the EDPs for the case of sliding and linear oscillators, respectively for the far-field and near-field record. Thus, independently of the degree of nonlinearity shown by the secondary oscillator, an accurate modeling of the seismic dynamics of both primary and secondary system is of key importance.

(2) The value of the viscous damping ratio significantly affects the peak response statistics of linear secondary systems vibrating close to the fundamental frequency of the primary structure. Indeed, increasing ζ_S from 0.02 to 0.05 resulted in a reduction in the response by about 50% for both earthquakes (close to the 40% reduction in the peak of the harmonic amplification factor, $D_S \cong 1/\zeta_S$).

(3) Peak response statistics of the sliding oscillator were found to be smooth functions of the sliding friction coefficient μ_s. For instance, increasing μ_s from 0.1 to 0.6 resulted in about 70% reduction in the expected value of the EDP.

(4) Reducing the slenderness angle and increasing the dynamic parameter was shown to exacerbate the tendency of the rocking oscillator to overturn. Interestingly, in comparison to other types of secondary oscillators, the strong nonlinearity of rocking block means that its seismic performance in terms of EPD is characterized by the highest value of coefficient of variation.

Future extensions of this work will include: (1) consideration of uncertainty in the structure in conjunction with uncertainty in the ground motion model and (2) investigation of other building types as well as further ground motion records. This will allow the development of an efficient framework for the stochastic response analysis of secondary structures.

References

[1] Taghavi S, Miranda E (2003): Response assessment of nonstructural building elements. *Technical Report PEER 2003/05*, Pacific Earthquake Engineering Research, Berkeley, USA.

[2] Villaverde R (2009): Fundamental concepts of earthquake engineering, Boca Raton, Fla, London.

[3] Muscolino G, Palmeri A (2007): An earthquake response spectrum method for linear light secondary substructures. *ISET Journal of Earthquake Technology*, **44**, 193-211.

[4] FIB (2012): Probabilistic performance-based seismic design. *Technical Report Bulletin 68*, International Federation for Structural Concrete, Lausanne, Switzerland.

[5] Giaralis A, Spanos P D (2009): Wavelet-based response spectrum compatible synthesis of accelerograms-Eurocode application (EC8). *Soil Dynamics and Earthquake Engineering*, **29**, 219-235.

[6] Cecini D, Palmeri A (2015): Spectrum-compatible accelerograms with harmonic wavelets. *Computers and Structures*, **147**, 26-35.

[7] Kanai K (1957): Semi-empirical formula for the seismic characteristics of the ground. *Technical Report 35*, University of Tokyo, Earthquake Research Institute.

[8] Tajimi H (1960): A statistical method of determining the maximum response of a building structure during an earthquake. *Proceedings of the 2nd World Conference on Earthquake Engineering*, Tokyo and Kyoto.

[9] Rezaeian S, Der Kiureghian A (2008): A stochastic ground motion model with separable temporal and spectral nonstationarities. *Earthquake Engineering & Structural Dynamics*, **37**, 1565-1584.

[10] Rezaeian S, Der Kiureghian A (2010): Stochastic modeling and simulation of ground motions for performance-based earthquake engineering. *Technical Report PEER 2010/02*, Pacific Earthquake Engineering Research, Berkeley, USA.

[11] Rezaeian S, Der Kiureghian A (2012): Simulation of orthogonal horizontal ground motion components for specified earthquake and site characteristics. *Earthquake Engineering & Structural Dynamics*, **41**, 335-353.

[12] Penzien J, Watabe M (1975): Characteristics of 3-dimensional earthquake ground motions. *Earthquake Engineering & Structural Dynamics*, **3**, 365-373.

[13] Menun C, Der Kiureghian A (1998): A replacement for the 30%, 40% and SRSS rules for multicomponent seismic analysis. *Earthquake Spectra*, **14**, 153-163.

[14] Rigato A B, Medina R A (2007): Influence of angle of incidence on seismic demands for inelastic single-storey structures subjected to bi-directional ground motions. *Engineering Structures*, **29**, 2593-2601.

[15] Kasinos S, Palmeri A, Lombardo M (2015): Performance-based seismic analysis of light SDoF secondary substructures. *12th International Conference on the Applications of Statistics and Probability in Civil Engineering*, Vancouver, Canada.

[16] Wen Y. K (1980): Equivalent linearization for hysteretic systems under random excitation. *Journal of Applied Mechanics*, **47**, 150-154.

[17] Ma F, Zhang H, Bockstedte A, Foliente G. C, Paevere P (2004): Parameter analysis of the differential model of hysteresis. *Journal of Applied Mechanics*, **71**, 342-349.

[18] Shenton H. W, Jones N. P (1991): Base excitation of rigid bodies I: Formulation. *Journal of Engineering Mechanics*, **117**, 2286-2306.

[19] Yim C. S, Chopra A. K, Penzien J (1980): Rocking response of rigid blocks to earthquakes. *Earthquake Engineering & Structural Dynamics*, **8**, 565-587.

[20] Zhang J, Makris N (2001): Rocking response of free-standing blocks under cycloidal pulses. *Journal of Engineering Mechanics*, **127**, 473-483.

[21] Palmeri A, Makris N (2008): Response analysis of rigid structures rocking on viscoelastic foundation. *Earthquake Engineering & Structural Dynamics*, **37**, 1039-1063.

[22] European Committee for Standardisation (2004): Eurocode 8, Design of structures for earthquake resistance.

[23] Computers and Structures (2007): SAP2000, Release 15.2.1, Berkeley.

[24] The MathWorks, Inc (2013): MATLAB, Release 8.2, Natick, Massachusetts, United States.